

# Heavy element nucleosynthesis in a collapsar

Shin-ichirou Fujimoto<sup>1</sup>, Masa-aki Hashimoto<sup>2</sup>, Kei Kotake<sup>3</sup>, and Shoichi Yamada<sup>3,4</sup>

## ABSTRACT

We investigate synthesis of heavy elements in a collapsar. We have calculated detailed composition of magnetically driven jets ejected from a collapsar, which is based on long-term, magnetohydrodynamic simulations of a rapidly rotating massive star of  $40M_{\odot}$  during core collapse. We follow evolution of abundances of about 4000 nuclides from the collapse phase to the ejection phase through the jet generation phase with use of two large nuclear reaction networks. We find that the  $r$ -process successfully operates in the jets, so that U and Th are synthesized abundantly when the progenitor has large magnetic field of  $10^{12}$  G and rapidly rotating core. Abundance pattern inside the jets is similar compared to that of  $r$ -elements in the solar system. Heavy neutron-rich nuclei  $\sim 0.01M_{\odot}$  can be ejected from the collapsar. The detailed abundances depend on nuclear properties of mass model,  $\beta$ -decay rate, and fission, for nuclei near the neutron drip line. Furthermore, we find that  $p$ -nuclei are produced without seed nuclei: not only light  $p$ -nuclei, such as  $^{74}\text{Se}$ ,  $^{78}\text{Kr}$ ,  $^{84}\text{Sr}$ , and  $^{92}\text{Mo}$ , but also heavy  $p$ -nuclei,  $^{113}\text{In}$ ,  $^{115}\text{Sn}$ , and  $^{138}\text{La}$ , can be abundantly synthesized in the jets. The amounts of  $p$ -nuclei in the ejecta are much greater than those in core-collapse supernovae (SNe). In particular,  $^{92}\text{Mo}$ ,  $^{113}\text{In}$ ,  $^{115}\text{Sn}$ , and  $^{138}\text{La}$  deficient in the SNe, are significantly produced in the ejecta.

*Subject headings:* Accretion, accretion disks — nuclear reactions, nucleosynthesis, abundances — stars: supernovae: general — MHD — methods: numerical — gamma rays: bursts

## 1. Introduction

A major fraction of elements heavier than iron are considered through a rapid neutron capture process ( $r$ -process) in an explosive event (e.g., Qian 2003, and references therein). Recent observations of metal poor stars (MPSs) have revealed that  $r$ -elements have been produced in an early phase of metal enrichment of the Galaxy (e.g., Truran et al. 2002). Abundance profiles of  $r$ -elements in some MPSs have similar patterns of the  $r$ -elements in the solar system. The fact may suggest that  $r$ -process can operate in a single site,

or sites with a similar condition. It should be noted that  $r$ -elements are likely to produce in a site, in which  $\alpha$  elements as well as iron group elements are not abundantly synthesized (Qian & Wasserburg 2003). Moreover, heavy  $r$ -elements (atomic number,  $Z > 50$ ) suggest to have different origin of light  $r$ -elements ( $Z > 40$ ) (Wasserburg et al. 1996).

Although various sites of  $r$ -process have been proposed, all the proposed scenarios have some deficiencies: (1) Neutrino-driven winds, which are launched from a new-born neutron star during core collapse of a massive star of  $10\text{-}25M_{\odot}$ , have been considered as a probable site of the  $r$ -process (e.g., Terasawa et al. 2002, and references therein). The scenario, however, requires an unlikely heavy and compact neutron star and the winds are possibly less abundant in heavy  $r$ -elements with mass number greater than 130 (Sumiyoshi et al. 2000). (2) It is suggested that  $r$ -process operates inside ejecta from an O-Ne-Mg core, which is produced in a final stage

<sup>1</sup>Department of Electronic Control, Kumamoto National College of Technology, Kumamoto 861-1102, Japan; fujimoto@ec.knct.ac.jp

<sup>2</sup>Department of Physics, School of Sciences, Kyushu University, Fukuoka 810-8560, Japan

<sup>3</sup>*Science & Engineering, Waseda University, 3-4-1 Okubo, Shinjuku, Tokyo 169-8555, Japan*

<sup>4</sup>*Advanced Research Institute for Science & Engineering, Waseda University, 3-4-1 Okubo, Shinjuku, Tokyo 169-8555, Japan*

of an  $8\text{-}10M_{\odot}$  star and is expected to explode promptly during the core collapse (Wheeler et al. 1998). The  $r$ -process is shown to operate during the explosion of the star if the explosion energy is an order of  $10^{50}\text{-}10^{51}$ ergs (Wanajo et al. 2003). However, the star reveals to explode very weakly with an explosion energy of  $2 \times 10^{49}$ ergs and an ejected mass of  $0.008M_{\odot}$ . Moreover, the ejected mass of the  $r$ -elements is possibly too high for  $r$ -elements in the Galaxy. (3) A small iron core of a presupernova star of  $\sim 11M_{\odot}$  is expected to explode promptly (e.g., Sumiyoshi et al. 2001). Ejecta from the core have enough low electron fraction, or neutron-rich, for  $r$ -process to operate successfully. The abundance profile of the ejecta can reproduce that of the solar system. However, it is still debatable to explode the core. (4)  $r$ -elements can be produced abundantly in a neutron-rich ejecta from the merger of two neutron stars (e.g., Freiburghaus et al. 1999). The composition is similar to that of the solar system. This scenario is, however, inconsistent to the  $r$ -element abundances of MPSs in light of the Galactic chemical evolution because of the rarity of the neutron star mergers (Argast et al. 2004). (5) Recently  $r$ -process calculations in MHD jets have been performed for a  $13M_{\odot}$  (Nishimura et al. 2005). Though the abundance distribution is well reproduced compared to the solar one, their results depend on the degree of neutronization that is very uncertain for multi-dimensional calculations.

On the other hands, any neutron capture processes cannot produce the  $p$ -nuclei that is 35 neutron deficient stable nuclei with mass number  $A \geq 74$ . The nuclei are considered to be synthesized by sequences of  $(\gamma, n)$  photodisintegrations of  $s$ -nuclei ( $s$ -process seeds) processed during helium core burning in a massive star. The scenario of the synthesis of the  $p$ -nuclei via the sequential photodisintegrations, or  $p$ -process, is proposed in the oxygen/neon layers of highly evolved massive stars during their presupernova phase (Arnould 1976) and during their supernova (SN) explosion (Woosley & Howard 1978). Extensive investigation of the  $p$ -process in core-collapse SNe has shown that the overall abundance profile of the  $p$ -nuclei reproduces that in the solar system (Rayet et al. 1995). The scenario, however, has conspicuous shortcomings (Rayet et al. 1995); (1) some  $p$ -

nuclei, such as  $^{92}\text{Mo}$ ,  $^{94}\text{Mo}$ ,  $^{96}\text{Ru}$ ,  $^{98}\text{Ru}$  and  $^{138}\text{La}$ , are underproduced compared with those in the solar system and (2) the ratio of  $p$ -nuclei to oxygen is smaller than that in the solar system.

During collapse of a massive star greater than  $35\text{-}40M_{\odot}$ , stellar core is considered to promptly collapse to a black hole (Woosley & Weaver 1995; Heger et al. 2003). When the star has sufficiently high angular momentum before the collapse, an accretion disk is formed around the hole and jets are shown to be launched from the inner region of the disk near the hole through magnetic processes (Proga et al. 2003; Fujimoto et al. 2006). Gamma-ray bursts (GRBs) are expected to be driven by the jets. This scenario of GRBs is called a collapsar model (Woosley 1993). Assisted by the accumulating observations implying the association between GRBs and the death of massive stars (e.g., Galama et al. 1998; Hjorth et al. 2003; Zeh, Klose, & Hartmann 2004), the collapsar model seems most promising. For accretion rates greater than  $0.1M_{\odot} \text{ s}^{-1}$ , the accretion disk is so dense and hot that nuclear burning is expected to proceed efficiently. In fact, an innermost region of the disk related to GRBs becomes neutron-rich through electron capture on nuclei (Beloborodov 2003; Pruet, Woosley & Hoffman 2003; Fujimoto et al. 2003b, 2004). Nucleosynthesis inside outflows from the neutron-rich disk has been investigated with steady, one-dimensional models of the disk and the outflows (Pruet, Woosley & Hoffman 2003; Pruet, Thompson & Hoffman 2004; Fujimoto et al. 2004, 2005). Not only neutron-rich nuclei (Fujimoto et al. 2004) but  $p$ -nuclei (Fujimoto et al. 2005) are shown to be produced inside the outflows. However, abundances of the outflows are shown to highly depend on electron fractions of the outflows. The electron fractions are expected to change during the generation phase of the outflows near the base of the outflows. Nevertheless, the electron fraction of the outflow at the base is assumed to be that of the disk at the base (Pruet, Thompson & Hoffman 2004; Fujimoto et al. 2004, 2005). Therefore, in order to evaluate change in the electron fractions of the outflows and to examine nucleosynthesis in a collapsar, we need non steady, multi-dimensional simulations of a collapsar from the collapsing phase of the star to the ejection phase of the outflows from the star.

In the present paper, we propose jets from a

collapsar, or rapidly rotating massive star during collapse to the black hole, as a *new r-process site*. In order to investigate heavy element synthesis in a collapsar, we have calculated detailed composition of magnetically-driven jets ejected from the collapsar, based on long-term, magnetohydrodynamic (MHD) simulations of a rapidly rotating, magnetized massive star of  $40M_{\odot}$  during core collapse, which has been performed in Fujimoto et al. (2006) recently. We follow evolution of the electron fraction and abundances of about 4000 nuclides from the collapse phase to the ejection phase through the jet generation phase, with the aid of two large nuclear reaction networks.

In §2 we briefly describe a numerical code for MHD calculation of the collapsing star, initial conditions of the star, and properties of jets from the star. In §3, we firstly present Lagrangian evolution of ejecta through the jets and then two large nuclear reaction networks, in which spontaneous and  $\beta$ -delayed fission is taken into account. It is also shown in §3 that *r*-process operates inside the jets and that *p*-nuclei that is deficient in core-collapse SNe can be produced inside the jets. We discuss effects on *r*-process of our assumptions in a later expansion phase of the ejecta and implications of collapsars for the Galactic chemical evolution of *r*-elements and *p*-elements in §4. Finally, we summarize our results in §5.

## 2. MHD Calculations of a Collapsar

We have carried out two-dimensional, Newtonian MHD calculation of the collapse of a rotating massive star of  $40M_{\odot}$ , whose core is assumed to be collapsed to a black hole promptly. We present our numerical models and results of the collapsar, in particular, the production and properties of jets.

### 2.1. Input Physics and Numerical Code

The numerical code for the MHD calculation employed in this paper is based on the ZEUS-2D code (Stone & Norman 1992). We have extended the code to include a realistic EOS (Kotake et al. 2004) based on the relativistic mean field theory (Shen et al. 1998). For lower density regime ( $\rho < 10^5 \text{g cm}^{-3}$ ), where no data is available in the EOS table with the Shen EOS, we use another EOS (Blinnikov et al. 1996). We consider neutrino cooling processes. The total neutrino cooling rate

is evaluated with a simplified neutrino transfer model based on the two-stream approximation (Di Matteo, Perna, & Narayan 2002), with which we can treat the optically thin and thick regimes on neutrino reaction approximately. We ignore resistive heating, whose properties are highly uncertain, not as in Proga et al. (2003). Spherical coordinates,  $(r, \theta, \phi)$  are used in our simulations and the computational domain is extended over  $50\text{km} \leq r \leq 10000\text{km}$  and  $0 \leq \theta \leq \pi/2$  and covered with  $200(r) \times 24(\theta)$  meshes. Fluid is freely absorbed through the inner boundary of 50km, which mimics a surface of the black hole, whose mass is continuously increased by the mass of the infalling gas through the inner boundary. We assume the fluid is axisymmetric and the mirror symmetry on the equatorial plane. We mimic strong gravity around the black hole in terms of the pseudo-Newtonian potential (Paczynski & Wiita 1980).

### 2.2. Initial conditions

We set the initial profiles of the density, temperature and electron fraction to those of the spherical model of a  $40M_{\odot}$  massive star before the collapse (Hashimoto 1995). The radial and azimuthal velocities are set to be zero initially, and increase due to the collapse induced by the central hole and self-gravity of the star. The computational domain is extended from the iron core to an inner oxygen layer and encloses about  $4M_{\odot}$  of the star. The boundaries of the silicon layers between the iron core and the oxygen layers are located at about 1800 km ( $1.88M_{\odot}$ ) and 3900km ( $2.4M_{\odot}$ ), respectively. We adopt an analytical form of the angular velocity  $\Omega(r)$  of the star before the collapse:

$$\Omega(r) = \Omega_0 \frac{R_0^2}{r^2 + R_0^2}, \quad (1)$$

as in the previous study of a collapsar (Mizuno, Yamada, Koide, & Shibata 2004a,b) and SNe (Kotake et al. 2004). Here  $\Omega_0$  and  $R_0$  are parameters of our model. Initial magnetic field,  $B_0$ , is assumed to be uniform, parallel to the rotational axis of the star. We consider case with  $\Omega_0 = 10 \text{rad s}^{-1}$ ,  $R_0 = 1000\text{km}$ , and  $B_0 = 10^{12}\text{G}$ , or case with a strongly magnetized progenitor whose core rotates rapidly, because we pay attention to nucleosynthesis of heavy elements, in particular *r*- and *p*-elements. As shown in later (§3.3), *r*-process can

operate successfully and some  $p$ -elements be synthesized in jets from the star during core collapse.

### 2.3. Properties of Jets

We briefly describe results of our MHD calculation (Fujimoto et al. 2006). Lagrangian evolution of physical quantities inside jets, which is important for nucleosynthesis, is shown in §3.1, in detail.

We find that jets can be magnetically driven from the central region of the star along the rotational axis; After material reaches to the black hole with high angular momentum of  $\sim 10^{17}\text{cm}^2\text{s}^{-1}$ , a disk is formed inside a surface of weak shock, which is appeared near the hole due to the centrifugal force and propagates outward slowly. The magnetic fields, which are dominated by the toroidal component, are chiefly amplified due to the wrapping of the field inside the disk and propagate to the polar region along the inner boundary near the black hole through the Alfvén wave. Eventually, the jets can be driven by the tangled-up magnetic fields at the polar region near the hole at  $t = 0.20\text{s}$ .

## 3. Nucleosynthesis in a collapsar

We examine nucleosynthesis in a collapsar, based on the results of our MHD simulations. We firstly show Lagrangian evolution of ejecta through jets in detail and then proceed nucleosynthesis inside the jets.

### 3.1. Lagrangian evolution of ejecta through jets

In order to calculate chemical composition of material inside jets, we need Lagrangian evolution of physical quantities, such as density, temperature, and, velocity of the material. We adopt a tracer particle method (Nagataki et al. 1997) to calculate the Lagrangian evolution of the physical quantities from the Eulerian evolution obtained our MHD calculations of a collapsar. Particles are initially placed from the Fe core to an inner O-rich layer. The numbers of the particles in a layer are weighted to the mass in the layer. The total numbers of the particles are set to be 1000, with which we can follow ejecta through the jets appropriately. We find that 59 particles can be ejected via the jets.

We have performed MHD calculation until  $t = t_f$  ( $t_f = 0.36\text{s}$ ). After  $t_f$ , we assume that particles are adiabatic and expand spherically and freely. Therefore, velocity, position, density, and temperature of a particle are set to be  $v(t) = v_0$ ,  $r(t) = r_f + v(t)(t - t_f)$ ,  $\rho(t) = \rho_f(r_f/r(t))^3$ ,  $T(t) = T_f(r_f/r(t))$ , respectively, where  $v_0$  is constant in time and set to be  $v_f$ . Here  $v_f$ ,  $r_f$ ,  $\rho_f$ , and  $T_f$  are velocity, position, density, and temperature of each particle at  $t_f$ , respectively. We briefly discuss how the assumption on the expansion affects abundance change in the expansion phase of the ejecta, later in §4.2.

Figure 1 shows trajectories of ejected particles with low  $Y_e$ , where  $Y_e$  is the electron fraction when the temperature of the particle is  $9 \times 10^9\text{K}$ . We find that the particles with low  $Y_e$  are initially located in the Fe core ( $\leq 1800\text{km}$ ). The trajectories of the particles are complex due to convective motion near the equatorial plane (Fujimoto et al. 2006).

Figure 2 shows the evolution of density and temperature. Initial density and temperature of a particle is set to be those of the presupernova in a layer where the particle is initially located. As the particle falls near the hole, the density and temperature increase. It should be emphasized that some particles become enough high densities ( $> 10^{10}\text{g cm}^{-3}$ ) and high temperatures ( $> 10^{10}\text{K}$ ) for protons to capture electrons, as we shall see later. For the particle of  $Y_e = 0.10$ , the density and temperature stay at high levels during  $t = 0.1\text{--}0.2\text{s}$  because of convection motion near the black hole (bottom panel in Figure 1). The motion is important for decrease in the electron fraction, as we shall see later (Figure 3).

### 3.2. Nuclear Reaction Network

As shown in Figure 2 (bottom panel), the ejecta can attain to high temperature greater than  $9 \times 10^9\text{K}$  near the black hole, where material is in nuclear statistical equilibrium (NSE). The abundances of the material in NSE can be expressed with simple analytical expressions (Clayton 1968; Qian 2003), which are specified by  $\rho$ ,  $T$ , and the electron fraction as in Fujimoto et al. (2003b). The electron fraction changes through electron and positron capture on nuclei. It should be emphasized that changes in the electron fraction through neutrino interactions can be ignored because the material is transparent for neutrinos

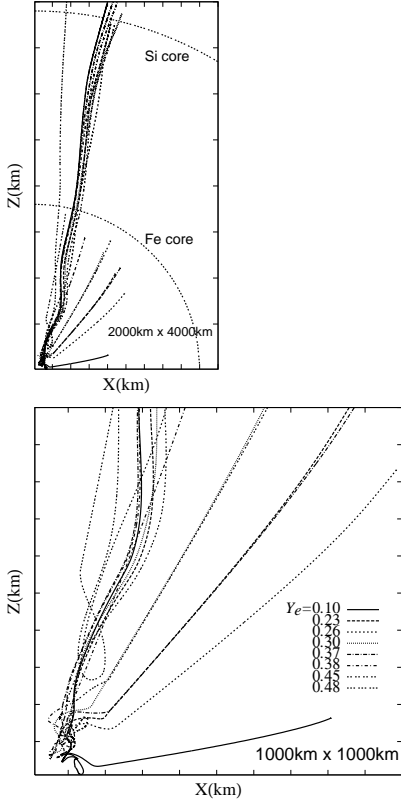


Fig. 1.— Trajectories of ejected particles. We select the particles to have various values of  $Y_e$ . The left and right panel cover the region of  $2000\text{km} \times 4000\text{km}$  and  $1000\text{km} \times 1000\text{km}$ , respectively.

even in the most dense part of the computational domain (Fujimoto et al. 2006).

In the relatively cool regime of  $T < 9 \times 10^9\text{K}$ , NSE breaks and the chemical composition is calculated with two large nuclear reaction networks, NETWORK A and NETWORK B, presented in Nishimura et al. (2005). The networks include about 4000 nuclei from neutron and proton up to Fermium, whose atomic number,  $Z$ , is 100 (see Table 1 in Nishimura et al. 2005). The networks contain reactions such as two and three body reactions, various decay channels, and electron-positron capture. The experimental masses and reaction rates are adopted if available. Otherwise, theoretical nuclear data, such as nuclear masses, rates of two body reactions, and  $\beta$ -decays are calculated with mass formula based on FRDM in NETWORK A but with that based in ETFSI in

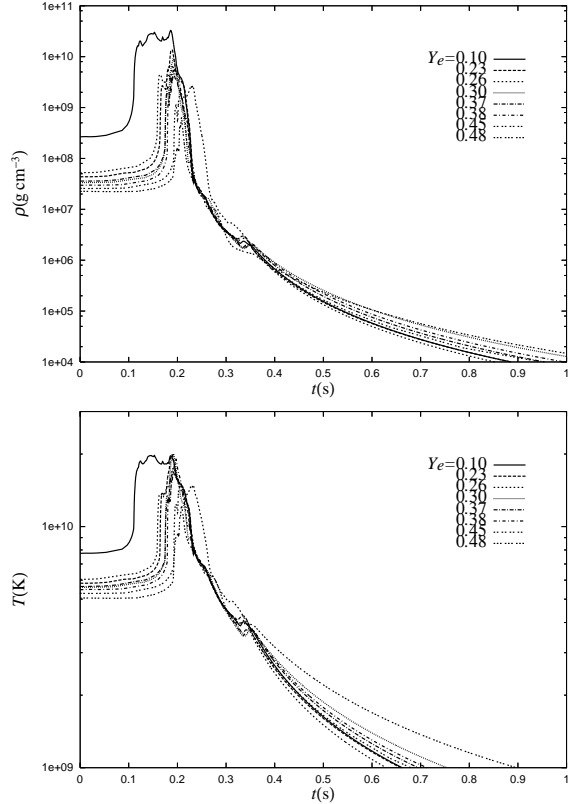


Fig. 2.— Evolution of density (top panel) and temperature (bottom panel) for the particles shown in Figure 1.

NETWORK B. We note that theoretical rates of two body reactions related to nuclei with  $Z \geq 93$  are same in the two network.

Spontaneous and  $\beta$ -delayed fission is taken into accounts in the both networks. Experimental half lives and branching ratios of the spontaneous fission are taken from Horiguchi, Tachibana, & Katakura (1996) and Kinsey et al. (1996). Theoretical formula of a half life (Kodama & Takahashi 1975, eq. (23)) with empirical fission barrier (Mamdouh, Pearson, Rayet & Tondeur 1999, 2001) is adopted for nuclei of  $Z < 100$  without experimental evaluation of the half live. We note that in Nishimura et al. (2005), the half lives through the spontaneous fission are set to be  $10^{-20}\text{s}$  for all nuclei with the mass number,  $A$ , greater than 254. Nuclei of  $Z = 100$  decay through sequences of  $\beta^-$  decays and/or fission. However, in our networks, the nuclei decay only through fission

because our networks contain nuclei up to  $Z = 100$  and the  $\beta^-$  channel of the nuclei of  $Z = 100$  shut off artificially. If we calculate the half life of the nuclei through the fission with the theoretical formula of Kodama & Takahashi (1975), the nuclei, whose half life is long compared with the duration of postprocessing calculation, cannot entirely decay. Therefore, for all nuclei of  $Z = 100$ , we tentatively set the half lives through the spontaneous fission to be  $10^{-20}$  s. We note that same branching ratios of  $\beta$ -delayed fission are taken from theoretical evaluation (Staudt & Klapdor-Kleingrothaus 1992) in the two networks although the theoretical ratios depend on an adopted mass formula (Panov et. al 2005). Empirical formula (Kodama & Takahashi 1975, eq.(5)) is adopted about decay products through the fission. We note that the distribution of fission yields is asymmetric.

### 3.3. Abundances of an ejected particle

Once we obtain the density and temperature evolution of a particle, we can follow abundance evolution of the particle during the infall and ejection, through post-processing calculation using the nuclear reaction network presented in the previous subsection. The ejected particles are initially located in the iron core (Figure 1). As the particles infall near the black hole, the particles become hotter than  $9 \times 10^9$  K, above which material in the particles is in NSE. We therefore switch to the NSE code from the nuclear reaction network to calculate abundance change of the particle. On the other hand, during the ejection, the temperature of the particles decreases and the particle becomes cooler than  $9 \times 10^9$  K. We switch back to the reaction network from the NSE code for the post-processing calculation of the particle composition. We perform the post-processing calculation of nucleosynthesis inside the jets until  $\sim 10^{10}$  yr. Therefore, almost unstable nuclei has been decayed to their corresponding stable nuclei.

Figure 3 shows evolution of the electron fraction for low  $Y_e$  particles. For  $t < 0.2$  s, the electron fractions decrease due to electron capture on nuclei, mainly protons, near the black hole, where density and temperature of the particles are high. On the other hands, for  $t > 0.4$  s, the electron fractions increase via  $\beta^-$ -decays of neutron-rich nuclei in particles with  $Y_e < 0.4$ . The fractions stay nearly constant values at  $0.2 \text{ s} < t < 0.4 \text{ s}$ ,

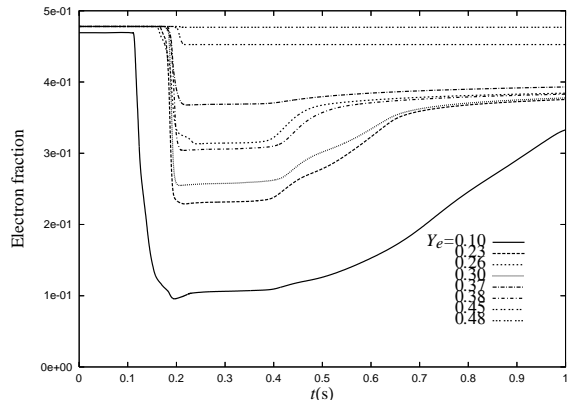


Fig. 3.— Evolution of the electron fraction for particles shown in Figure 1.

at which the particles are abundant in neutrons and long lived nuclei with the neutron number around 50.  $\beta$ -decay processes are therefore less important for decrease in the electron fraction at  $0.2 \text{ s} < t < 0.4 \text{ s}$ . We find that there exist particles with  $Y_e$  lower than 0.3. The particles can be so neutron-rich that  $r$ -process operates efficiently. Not only a region of high density and temperature but also staying in the region for a long time due to convective motion (Figure 1) are required for significant decrease in the electron fraction of the particles. The particle of low  $Y_e \sim 0.1$  has low entropy per baryon ( $\sim 10\text{-}20 k_B$ ) where  $k_B$  is the Boltzmann constant. The condition is similar to that of ejecta from a massive star of  $\sim 11 M_\odot$ , in which the stellar material is expected to be exploded promptly during SN explosion (Sumiyoshi et al. 2001). The similar condition is also realized in a jet-like explosion from an inner core of a rotating star of  $13 M_\odot$  (Nishimura et al. 2005). The  $r$ -process can operate in the explosion (Nishimura et al. 2005) but the minimum  $Y_e$  in the explosion ( $= 0.158$ ) is higher than that in the present study ( $= 0.10$ ). Therefore, U and Th cannot be synthesized abundantly in the explosion, not as in the present study, as we shall see later (Figure 12).

We have adopted weak interaction rates as those in Fuller, Fowler, & Newman (1980, 1982). However, recent shell-model calculations of the rates (Langanke et al. 2003) for nuclei in the mass range  $A = 45\text{-}65$  have resulted in substantial revisions to the old rate set of Fuller, Fowler, & Newman (1980, 1982). In order to estimate the effects

of the revisions on  $Y_e$  of particles, we have calculated evolution of the electron fraction of the  $Y_e = 0.10$  particle using the revised weak interaction rates. We find that the electron fraction calculated with the revised rates is slightly larger than that with the old rates. However, the difference in  $Y_e$  with the two rate sets is only up to two percents. This is because electrons are dominantly captured by protons and the rates of electron capture on protons are comparable between the two sets of the rates in high temperature and high density regimes.

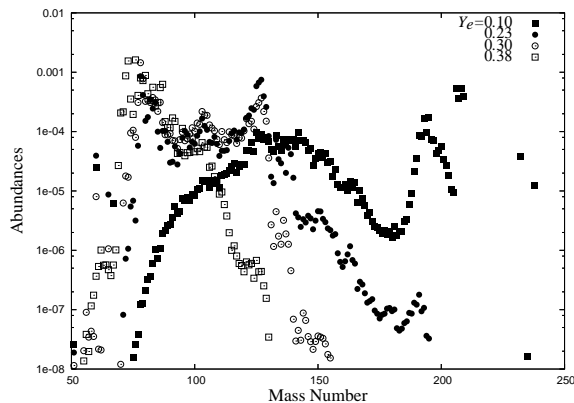


Fig. 4.— Abundances of nuclei with respect to the mass number  $A$  for particles with low  $Y_e$ . Filled squares, filled circles, open circles, and open squares represent the abundances of particles with  $Y_e = 0.10, 0.23, 0.30,$  and  $0.38$ , respectively.

Figure 4 shows abundances of nuclei with respect to  $A$  for particles with  $Y_e = 0.10, 0.23, 0.30,$  and  $0.38$  using NETWORK B. For a lower  $Y_e$  particle, the particle becomes more neutron-rich in the NSE phase, and the abundances of heavier nuclei increase. We find that the second-peak nuclei ( $A \sim 130$ ) and the third-peak nuclei ( $A \sim 195$ ) can be abundantly produced in particles with  $Y_e$  less than  $0.3$  and  $0.1$ , respectively. We also find that the particle with  $Y_e = 0.10$  is abundant in U and Th. The particle has enough low  $Y_e$  for rapid neutron capture to proceed efficiently. We find that the nuclear flow on the nuclear chart proceeds near the neutron drip line and heavy neutron-rich nuclei with  $Z \geq 95$  are abundantly synthesized in the particle (Figure 5). Therefore, nuclear properties of mass model,  $\beta$ -decay, and fission, for nuclei near the drip line are important for abundance calcula-

tion of the  $Y_e \sim 0.1$  particle.

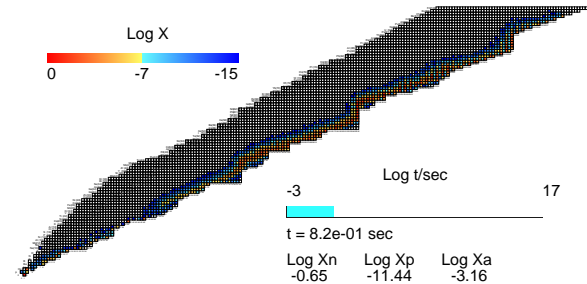


Fig. 5.— Mass fractions on the nuclear chart for a particle with  $Y_e = 0.10$  at  $t = 0.82$  s calculated with NETWORK B.

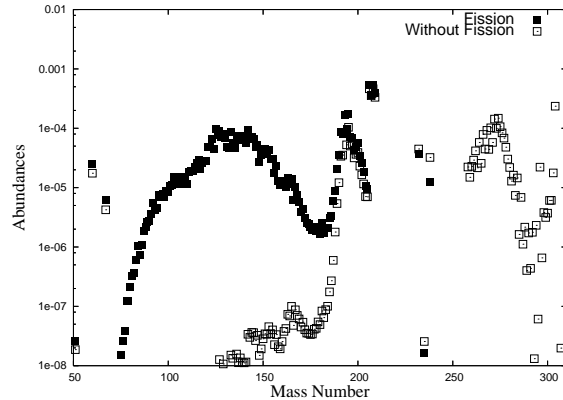


Fig. 6.— Abundances of the particle with  $Y_e = 0.10$  calculated with NETWORK B (filled squares) and a network same as NETWORK B but ignored all fission processes (open squares).

We have taken into accounts spontaneous and  $\beta$ -delayed fission in our nuclear reaction networks. Fission is expected to have important role in the composition of particles with low  $Y_e$ . Figure 6 shows the abundances of the particle with  $Y_e = 0.10$  calculated with NETWORK B and a network same as in NETWORK B but ignored all fission processes. We find that the abundances of nuclei with  $A > 250$  as well as those with  $60 < A < 180$  change significantly if the fission processes are ignored. This is due to decay through fission and fission yields, whose mass numbers are abundantly distributed in  $60 < A < 180$ . We note that fission recycling cannot take place in the particle.

Finally, in order to see dependence of particle

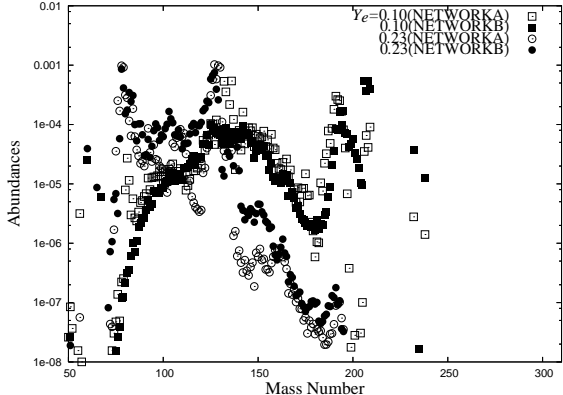


Fig. 7.— The abundances of particles with  $Y_e = 0.10$  and  $0.23$  calculated with NETWORK A and B presented in §3.2. Open squares, filled squares, open circles, and filled circles represent abundances of the particle with  $Y_e = 0.10$  (NETWORK A), those with  $Y_e = 0.10$  (NETWORK B), those with  $Y_e = 0.23$  (NETWORK A), and those with  $Y_e = 0.23$  (NETWORK B), respectively.

composition on a nuclear mass model, we present the composition of particles with  $Y_e = 0.10$  and  $0.23$  using NETWORK A and B in Figure 7. We find that overall abundance profiles are similar for the two networks for the both particles. Detailed profiles are, however, rather different for the two networks. For the  $Y_e = 0.10$  particle, it is remarkable that heavy elements, such as Pb, Th, and U, with NETWORK B are more abundant than NETWORK A.

The time-scale of a reaction sequence, which synthesizes heavy neutron-rich nuclei greater than  $A > 200$ , mainly depends on half lives of the waiting-point nuclei of  $r$ -process, whose neutron number,  $N$ , is 82 or 126 and half life is long compared to the ejection time-scale of the particle. The half lives based on FRDM are shorter than those with ETFSI by an order of magnitude for nuclei with lower atomic number (Figure 8), such as  $^{124}\text{Mo}$  ( $N = 82$ ) and  $^{190}\text{Gd}$  ( $N = 126$ ), which are abundantly synthesized. Hence, successive neutron capture can proceed to synthesize heavy neutron-rich nuclei with  $A > 250$  in NETWORK A. Most of nuclei with  $A > 250$  decay to not U and Th but lighter nuclei via fission (Figure 6). Small fractions of the nuclei decay to U and Th through successive  $\beta$ -decays firstly followed by

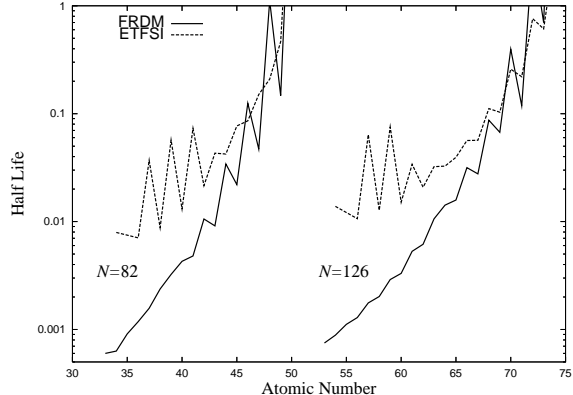


Fig. 8.— Half lives of neutron-rich nuclei with  $N = 82$  and  $126$ . The half lives are calculated with the two mass models base on FRDM (solid lines) and ETFSI (dashed lines).

$\alpha$ -decays. On the other hand, neutron-rich nuclei with  $A = 232, 235,$  and  $238$ , can be abundantly produced in the ejecta with NETWORK B. Most of the nuclei decay to U and Th through  $\beta$ -decays. Small fractions of neutron-rich nuclei with  $A > 250$  also decay to U and Th via a similar sequence of  $\beta$  and  $\alpha$ -decays as in case with NETWORK A. This is because U and Th are underproduced in the ejecta with NETWORK A compared to those with NETWORK B.

### 3.4. Integrated abundances

We shall move on mass-weighted abundances in the ejecta through the jets.

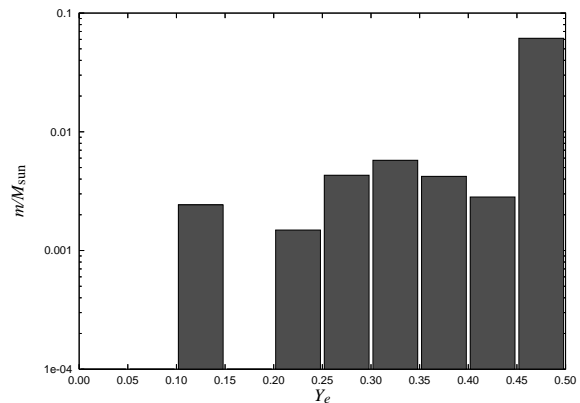


Fig. 9.— Mass distribution with respect to  $Y_e$  in ejecta.



Figure 9 shows mass distribution with respect to  $Y_e$  in the ejecta. The ejected mass is  $0.081M_\odot$  through the jets. We find that most particles have high  $Y_e > 0.45$ , whose mass is  $0.061M_\odot$ , and that masses of particles in which third-peak nuclei can be produced ( $Y_e \sim 0.1$ ) are  $2.4 \times 10^{-3}M_\odot$ . Masses of particles with  $Y_e \leq 0.4$  are  $1.8 \times 10^{-2}M_\odot$ .

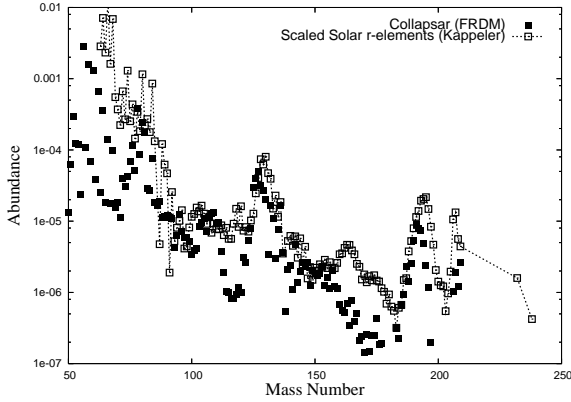


Fig. 10.— Integrated abundances in ejecta calculated with NETWORK A. Filled squares and open squares with dotted line represent abundances of the collapsar and  $^{153}\text{Eu}$ -scaled abundances of solar  $r$ -elements (Käppeler et al. 1989), respectively.

Figure 10 shows mass weighted-abundances in the ejecta calculated with NETWORK A with respect to the mass number. The abundances of the solar  $r$ -elements (Käppeler et al. 1989) are also presented in Figure 10. We scale the abundances in the ejecta with the abundance of  $^{153}\text{Eu}$  because most Eu, up to 94.2%, is produced via  $r$ -process in the solar system (Arlandini et al. 1999). We find that the abundances in the jets well reproduce the solar pattern of  $r$ -elements. It is clearly seen that nuclei around the second ( $A \sim 130$ ) and third ( $A \sim 195$ ) peaks can be synthesized in the ejecta via the jets. However, nuclei with  $160 < A < 180$  are underproduced compared with those in the solar system because of the lack of a  $Y_e = 0.15\text{--}0.20$  particle (Figure 9). Nuclei with  $A < 70$  are also less abundant due to low  $Y_e$  of the particles.

Figure 11 shows mass weighted-abundances in the ejecta calculated with NETWORK A with respect to  $Z$  and the Eu ( $Z = 63$ )-scaled abundances of the solar  $r$ -elements (Burris et al. 2000). An appreciable amount of  $r$ -elements of  $Z \geq 40$  can be produced inside the jets. The abundances

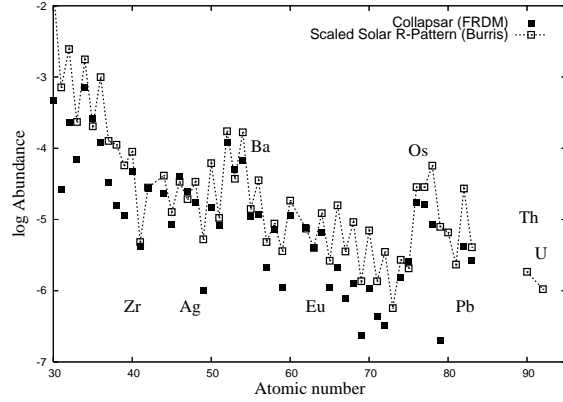


Fig. 11.— Integrated abundances in ejecta calculated with NETWORK A. Filled squares and open squares with dotted line represent abundances of the collapsar and Eu( $Z = 63$ )-scaled abundances of solar  $r$ -elements (Burris et al. 2000), respectively.

of the jets well reproduce those in the solar system. However, the detailed abundance profile of the ejecta are rather different from that of the solar  $r$ -elements. Elements with  $65 \leq Z \leq 73$  and  $79 \leq Z \leq 81$  are underproduced. U and Th are also underproduced inside the jets.

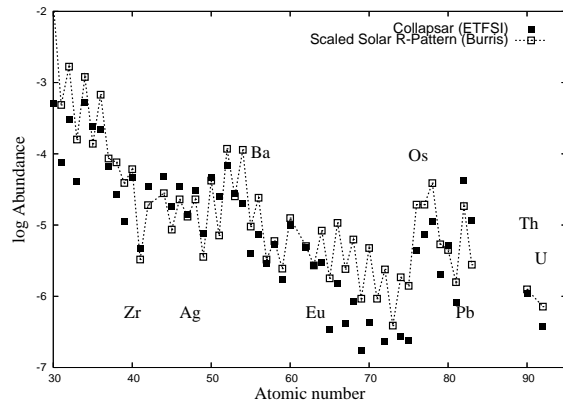


Fig. 12.— Same as Fig. 11 but with NETWORK B.

If we use the another network, or NETWORK B, mass weighted-abundances in the ejecta slightly change but the overall profile is not largely different from those with NETWORK A (Figure 12). The abundances of the jets well reproduce those in the solar system, other than the ranges of  $Z < 40$

and  $70 \leq Z \leq 75$ , in which the jet abundances are underproduced compared with those in the solar system. It should be noted that U and Th, which are underproduced with NETWORK A, are comparably produced as the solar system.

### 3.5. Abundances of nuclei other than $r$ -process elements

We present abundances of nuclei other than  $r$ -elements. Note that our computational domain of MHD calculation extends over an oxygen rich layer ( $\leq 10000\text{km}$ ). Ejecta from an outer oxygen rich layer are not taken into account. Ejected masses are therefore under-estimated of elements lighter than iron, in particular  $\alpha$ -elements.

#### 3.5.1. $\alpha$ - and iron group elements

As shown in Figure 9, most particles of  $0.061M_{\odot}$  have high  $Y_e > 0.45$ . Inside particles with  $Y_e \sim 0.5$ ,  $\alpha$ -rich freezeout takes place as in the ejecta via a core-collapse SN.  $^{56}\text{Ni}$ , which decays to  $^{56}\text{Fe}$ , is therefore abundantly produced inside the ejecta. We find that  $^{56}\text{Fe}$  amounts to  $0.013M_{\odot}$ , which is comparable to masses of  $^{28}\text{Si}$  ( $0.013M_{\odot}$ ),  $^{32}\text{S}$  ( $9.4 \times 10^{-3}M_{\odot}$ ),  $^{58}\text{Ni}$  ( $7.0 \times 10^{-3}M_{\odot}$ ), and  $^{60}\text{Ni}$  ( $6.4 \times 10^{-3}M_{\odot}$ ). Inside particles with  $Y_e$  slightly lower than 0.5, or  $\sim 0.49$ , nuclei heavier than iron, such as  $^{62,64}\text{Ni}$ ,  $^{64,66,68}\text{Zn}$ , and  $^{78}\text{Se}$ , can be produced to be greater than  $5 \times 10^{-4}M_{\odot}$ .

#### 3.5.2. $p$ -elements

We shall examine abundances and synthesis of  $p$ -nuclei in the ejecta through the jets. It is suggested that  $p$ -nuclei are produced inside an accretion disk with high mass accretion rates, which can be realized during the collapse of a rotating massive star (Fujimoto et al. 2003a).

We find that  $p$ -nuclei are significantly synthesized in the ejecta in spite of neutron-richness of the ejecta. Figure 13 shows the mass fractions of  $p$ -nuclei abundantly produced in the ejecta. The abundances are calculated with NETWORK B. The fractions are normalized by those in the solar system (Anders & Grevesse 1989). We also show mass fractions of  $p$ -nuclei from core-collapse SNe averaged over an initial mass function (Rayet et al. 1995). We find that not only light  $p$ -nuclei, such as  $^{74}\text{Se}$ ,  $^{78}\text{Kr}$ ,  $^{84}\text{Sr}$ , and  $^{92}\text{Mo}$ , but also heavy

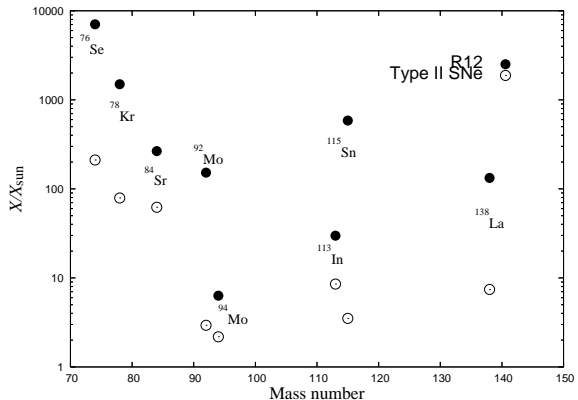


Fig. 13.— Mass fractions of  $p$ -nuclei abundantly produced in the ejecta through the jets. The fractions are normalized by those in the solar system (Anders & Grevesse 1989). IMF averaged abundances of  $p$ -nuclei from core-collapse SNe (Rayet et al. 1995) are shown with open circles.

$p$ -nuclei,  $^{113}\text{In}$ ,  $^{115}\text{Sn}$ , and  $^{138}\text{La}$ , are produced in the ejecta abundantly. The abundances of  $p$ -nuclei in the ejecta are much greater than those in core-collapse SNe (Rayet et al. 1995). It should be emphasized that  $^{92}\text{Mo}$ ,  $^{113}\text{In}$ ,  $^{115}\text{Sn}$ , and  $^{138}\text{La}$ , which are deficient in core-collapse SNe (Rayet et al. 1995), are significantly produced in the ejecta. We note that if we use NETWORK A, the abundances of heavy  $p$ -nuclei,  $^{113}\text{In}$ ,  $^{115}\text{Sn}$ , and  $^{138}\text{La}$ , decrease by a factor of 2, 8, and 8, respectively.

In order to see production mechanism of the light  $p$ -nuclei, we present abundance evolution in a tracer particle with  $Y_e = 0.48$  in Figures 14. We note that the particle corresponds to the particle with  $Y_e = 0.48$  in Figure 1-3. As the particle infalls near the black hole, the temperature raises up to  $1.21 \times 10^{10}\text{K}$  (Figure 2). Heavy nuclei are destroyed through photodisintegration as the temperature increases. Abundances are rapidly enhanced of proton, neutron, and  $^4\text{He}$ . As the temperature decreases during the ejection of the particle through the jets, heavy elements are re-assembled through neutron capture firstly, and then proton and  $\alpha$  capture. We find that the light  $p$ -nuclei,  $^{74}\text{Se}$ ,  $^{78}\text{Kr}$ ,  $^{84}\text{Sr}$ , and  $^{92}\text{Mo}$  are produced via sequences of proton capture; For  $^{92}\text{Mo}$ , abundances are enhanced through a reaction sequence,  $^{86}\text{Kr}(p,\gamma)^{87}\text{Rb}(p,\gamma)^{88}\text{Sr}(p,\gamma)^{89}\text{Y}(p,\gamma)^{90}\text{Zr}(p,\gamma)^{91}\text{Nb}(p,\gamma)^{92}\text{Mo}$ .

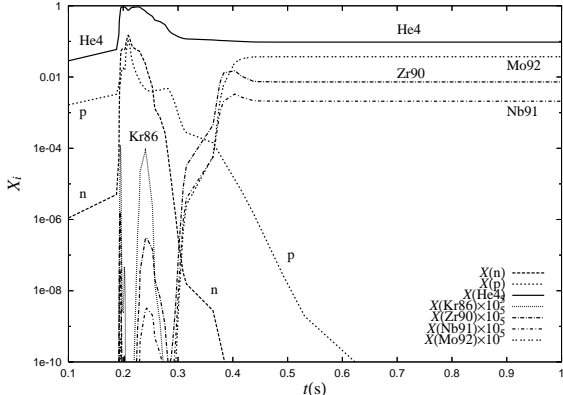


Fig. 14.— Abundance evolution of a tracer particle with  $Y_e = 0.48$ . Mass fractions are shown of  $^{86}\text{Kr}$ ,  $^{90}\text{Zr}$ ,  $^{91}\text{Nb}$ , and  $^{92}\text{Mo}$ , whose abundances are multiplied by  $10^5$ . Fractions are also presented of proton, neutron, and  $^4\text{He}$ .

Note that  $^{86}\text{Kr}$ , whose neutron number is equal to the magic number of 50, are abundantly synthesized through neutron-capture because of neutron-richness of the particle ( $Y_e = 0.48$ ). The reaction sequences, which produce the light  $p$ -nuclei, have been suggested to be realized in SNe (Howard et al. 1991).

On the other hands, the heavy  $p$ -nuclei,  $^{113}\text{In}$ ,  $^{115}\text{Sn}$ , and  $^{138}\text{La}$ , have different production mechanism as the light  $p$ -nuclei. We find that the heavy  $p$ -nuclei can be produced only in a particle with  $Y_e = 0.10$  and through fission processes. In fact, the heavy  $p$ -nuclei cannot be synthesized if we ignore all decay channel through fission (Figure 6).  $^{138}\text{La}$  are produced through fission directly but  $^{113}\text{In}$  and  $^{115}\text{Sn}$  are  $\beta$ -decay products of fission yields,  $^{113}\text{Cd}$  and  $^{115}\text{In}$  (and their  $\beta^-$ -decay parents), respectively, whose half lives are  $9.3 \times 10^{15}$  yr and  $4.4 \times 10^{14}$  yr. We have performed the post-processing calculation of nucleosynthesis inside the jets until  $\sim 10^{10}$  yr. If the calculation is performed for a much shorter time, say  $\sim 10^8$  yr, the abundances are found to decrease by about two orders of magnitude. It should be noted that we have adopted the empirical asymmetric distribution of fission yield (Kodama & Takahashi 1975), which can be fit experimental yields but its extrapolation into experimentally unknown region is questionable (Kodama & Takahashi 1975). The abundances of the heavy  $p$ -nuclei are therefore highly

uncertain.

## 4. Discussion

### 4.1. Neutrino effects on nucleosynthesis

We have ignored changes in the electron fraction through (anti-)neutrino capture on nuclei. This is because the material is transparent for neutrinos even in the most dense part of the computational domain, as shown in the previous study (Fujimoto et al. 2006). We have considered the collapse of a massive star to the black hole. Neutrino emission is therefore found to be smaller than that in cases of core collapse to a neutron star (Fujimoto et al. 2006) because of lower neutrino emission from the region near the black hole compared with that near the neutron star. Hence, jets from a collapsar are likely to be an appropriate site of the  $r$ -process because of low electron fraction and high neutron-richness due to low neutrino emission.

### 4.2. Abundance change in an expansion phase

As shown in Figure 5, rapid neutron capture takes place during a later phase, or  $t > 0.5$  s, which is greater than  $t_f = 0.36$  s. Evolution of physical quantities in the phase is described in terms of that of adiabatic free expansion. In order to estimate dependence of particle composition on the assumption at the phase, we calculate abundances of a particle with  $Y_e = 0.10$  for various expansion velocities in the later phase (§3.1). The kinetic energy of the jets is larger than the internal and magnetic energies (Table 1). Therefore, the velocity of the jets is unlikely to change appreciably if the jets are adiabatic. Figure 15 shows the abundances for cases with  $v_0 = v_f$ ,  $v_0 = 2v_f$ , and  $v_0 = 0.5v_f$ , which are represented with filled squares, open triangles, and, open circles, respectively. For slower particles, neutron capture proceeds more efficiently. Nuclei with  $A \sim 170$  are less abundant but those with  $A \sim 190$  are enhanced compared with those in a faster particle. Nuclei heavier than U and Th are abundantly produced and eventually decay through fission. However, the abundances are similar for three cases. We conclude that the particle composition weakly depends on the assumption on the later phase expansion.

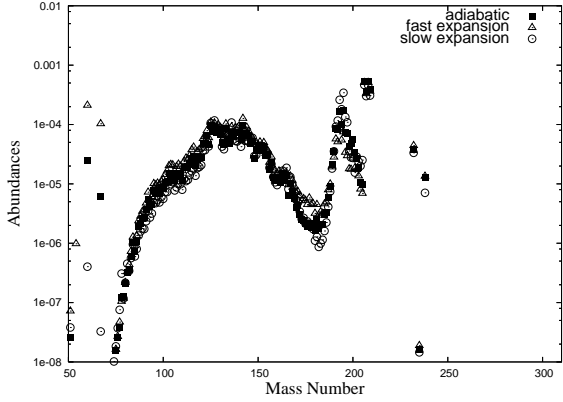


Fig. 15.— Abundances of the particle with  $Y_e = 0.10$  for various expansion velocities in the later phase. Filled squares, open triangles, and, open circles represent abundances of the particle for  $v_0 = v_f$ ,  $v_0 = 2v_f$ , and  $v_0 = 0.5v_f$ , respectively.

### 4.3. Implications for Galactic chemical evolution

#### 4.3.1. *r*-elements

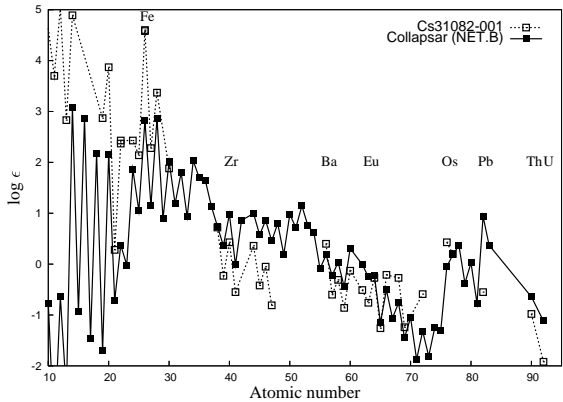


Fig. 16.—  $\log \epsilon$  of the ejecta via the jets (open circles with dotted line) and CS31082-001 (filled circles with solid line). Note that  $\log \epsilon$  are not scaled in the panel.

Figure 16 shows  $\log \epsilon_i$ <sup>1</sup> for element  $i$  of the ejecta through the jets, which are assumed to be uniformly mixed into inter stellar medium (ISM) of mass,  $M_{\text{ISM}} = 4 \times 10^5 M_{\odot}$ . Note that  $M_{\text{ISM}} =$

<sup>1</sup> $\log \epsilon_A = \log(N_A/N_H) + 12$  and  $[A/B] = \log(N_A/N_B) - \log(N_A/N_B)_{\odot}$  for elements A and B.

$4 \times 10^5 M_{\odot}$  is slightly larger than mass of ISM polluted by an SN with the explosion energy of  $10^{51}$  ergs (Shigeyama & Tsujimoto 1998). Observed  $\log \epsilon_i$  in an extremely metal poor star, CS31082-001 ( $[\text{Fe}/\text{H}] = -2.9$ ), is also presented in Figure 16. We find that  $\log \epsilon_i$  of ISM mixed with the ejecta are similar to those in CS31082-001 for  $Z \geq 38$ . However, for  $Z < 30$ ,  $\log \epsilon_i$  of the ISM are much less than those in CS31082-001. Especially, iron is poor in the ISM mixed with the ejecta compared with that in CS31082-001 ( $[\text{Fe}/\text{H}] \sim 5$  of the ISM).

Moreover, we find that the observed  $\log \epsilon_i$  of CS31082-001 is well reproduced with those of the material in ISM for elements with  $Z$  ranging from 10 to 92. (Figure 17), if we assumed that the ejecta via the jets is uniformly mixed to the ISM of  $M_{\text{ISM}}$ , which is pre-enriched by a hypernova (HN) of  $40 M_{\odot}$ . The ejected masses of nuclei from the HN are taken from model 40C in Maeda & Nomoto (2003), in which the star explodes aspherically with extremely high explosion energy of  $3.23 \times 10^{52}$  erg and ejects massive  $^{56}\text{Ni}$  of  $0.24 M_{\odot}$ . We note that nickel is over abundant if we adopt masses of SN ejecta of a star, which explodes spherically and can ejecta massive iron.

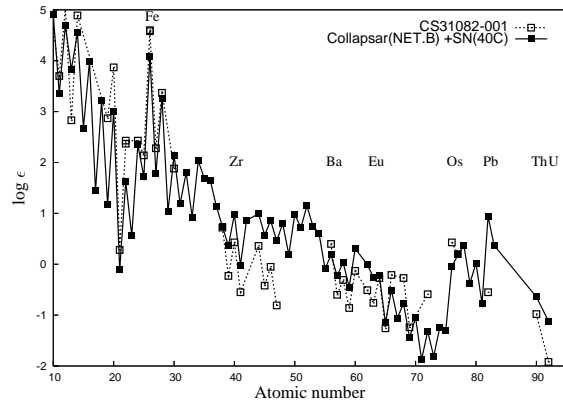


Fig. 17.— Same as Fig. 16 but for the ejecta via the jets mixed with ejecta via a hypernova of  $40 M_{\odot}$ .

#### 4.3.2. *p*-elements

The ejected mass from the collapsar is  $0.081 M_{\odot}$ . The mass is smaller than ejected mass of *p*-nuclei,  $M_{\text{PPL}}$ , of  $0.15 M_{\odot}$  from a core-collapse SN of  $13 M_{\odot}$  (Rayet et al. 1995). However, the

$p$ -nuclei,  $^{74}\text{Se}$ ,  $^{78}\text{Kr}$ ,  $^{84}\text{Sr}$ ,  $^{92}\text{Mo}$ ,  $^{113}\text{In}$ ,  $^{115}\text{Sn}$ , and  $^{138}\text{La}$ , are produced much abundantly in the ejecta from the collapsar by 1-2 orders of magnitude compared with those in the ejecta from the SN (Figure 13). The masses of the above  $p$ -nuclei from the collapsar, therefore, are comparable or greater than those from the SN. The collapsar could be important for the Galactic chemical evolution of the  $p$ -nuclei if the events are not rare compared with core-collapse SNe.

Moreover,  $p$ -process in oxygen-rich layers is also expected to operate in the collapsar, as in  $p$ -process layers (PPLs) in core-collapse SNe. This is because  $s$ -process seeds of  $p$ -process exist in the layers due to weak  $s$ -process during He core burning of the star and the jets propagate in the layers to heat the layers to enough high temperatures for  $p$ -process to operate efficiently. Therefore masses of  $p$ -nuclei can be enhanced via the  $p$ -process. Ejected  $p$ -nuclei from the collapsar are the sum of those in the ejecta from oxygen-rich layers with the composition similar to that in PPLs in core-collapse SNe and those in the jets from inner core, which abundantly contain  $p$ -nuclei deficient in the SNe.

Although ejected mass of  $p$ -nuclei is possibly smaller than  $M_{\text{PPL}}$  because of aspherical explosion in the collapsar, a ratio of the mass to ejected mass of oxygen can be much larger than a ratio in the SNe. This is because the jets from the inner core have small amounts of oxygen. We note that the ratio in the SNe is problematically much smaller compared with that in the solar system (Rayet et al. 1995).

#### 4.3.3. Event rates

Finally, we briefly discuss on event rates of GRBs linked to the death of a massive star and jet-like explosion related to GRBs. A current GRB rate is estimated to be  $\sim 5 \times 10^{-5} \text{ yr}^{-1}$  in the Milky Way (Firmani et al. 2004). A GRB rate in an average galaxy is comparable to that in the Galaxy and is much smaller than the rate of core-collapse SNe by a factor of several hundreds (Podsiadlowski et al. 2004). The GRB rate is however sensitive to the jet opening angle (Podsiadlowski et al. 2004). The rate rapidly increases at red shift  $z \sim 1$  and is gradually enhanced at higher red shift (Yonetoku et al. 2004; Murakami et al. 2005). However, an estimated star formation rate is constant at higher

red shift, though the rate increases at  $z \sim 1$  as the GRB rate (Giavalisco et al. 2004). Thus, the relative GRB rate to core-collapse SNe enlarges at the higher  $z$ .

Moreover, the jets in the current investigation are too slow ( $\leq 0.1c$ ) and heavy ( $0.022M_{\odot}$ ) to induce GRB. Although this “failed GRB” is possibly hard to observe compared with normal GRBs, two failed GRBs are suggested to be associated with Type Ic SNe, SN2001em (Granot & Ramirez-Ruiz 2004) and SN2002ap (Totani 2003). A ratio of failed GRBs to Type Ic SNe is estimated to be  $2/40 = 5\%$  for nearby 40 Type Ibc SNe (Granot & Ramirez-Ruiz 2004). Note that the ratio can be much greater than the above estimate, or  $2/15 = 13.3\%$  if samples of Type Ibc SNe are limited to those with late-time ( $> 100$  s) observations, or 15 Type Ibc SNe (Granot & Ramirez-Ruiz 2004). Accordingly, we can estimate a failed GRB rate to  $\sim 1.3 \times 10^{-4} \text{ yr}^{-1}$  with an estimate of a Type Ibc rate of  $1 \times 10^{-3} \text{ yr}^{-1}$  (Podsiadlowski et al. 2004). Therefore, failed GRBs are possibly more frequent than normal GRBs.

In brief, the jets from the failed GRBs have much importance to chemical evolution of galaxies compared to normal GRBs because of greater ejection mass and frequency. In the early universe, or  $z > 1$ , the jets could have a significant contribution to chemical evolution of galaxies, in particular heavy elements, which cannot be abundantly synthesized in core-collapse SNe.

## 5. Summary and Conclusions

We have calculated detailed composition of magnetically-driven jets ejected from a collapsar, based on long-term, magnetohydrodynamic simulations of a rapidly rotating massive star of  $40M_{\odot}$  during core collapse. The magnetic field of the star before the collapse is set to be uniform and parallel to the rotational axis of the star. We consider case with the magnetic field of  $10^{12}$  G. We follow evolution of abundances of about 4000 nuclei from the collapse phase to the ejection phase through the jet generation phase with the aid of a NSE code and two large nuclear reaction networks. We summarize our conclusions as follows;

1. The  $r$ -process successfully operates in the jets. Abundances of the jets have similar profile as those of  $r$ -elements in the solar

system, though the detailed abundances are different. U and Th can be abundantly synthesized in the jets.

2. Massive neutron-rich nuclei  $\sim 0.01M_{\odot}$  can be ejected from the collapsar.
3. The abundances highly depend on nuclear properties of mass model,  $\beta$ -decay and fission, for nuclei near the neutron drip line.
4. Fission is important for abundances of nuclei with not only  $A > 250$  but  $60 < A < 180$ .
5. Light  $p$ -nuclei, such as  $^{74}\text{Se}$ ,  $^{78}\text{Kr}$ ,  $^{84}\text{Sr}$ , and  $^{92}\text{Mo}$ , are abundantly produced in the ejecta due to successive proton capture. Heavy  $p$ -nuclei,  $^{113}\text{In}$ ,  $^{115}\text{Sn}$ , and  $^{138}\text{La}$ , are abundantly synthesized in the jets through fission.
6. The abundances of  $p$ -nuclei in the ejecta are much greater than those in core-collapse SNe, in particular,  $^{92}\text{Mo}$ ,  $^{113}\text{In}$ ,  $^{115}\text{Sn}$ , and  $^{138}\text{La}$ , which are deficient in the SNe, are significantly produced in the ejecta.
7. If we assumed that the ejecta via the jets is uniformly mixed to the ISM of  $4 \times 10^5 M_{\odot}$ , which is pre-enriched by a hypernova of  $40M_{\odot}$ ,  $\log \epsilon_i$  of the material in the ISM well reproduces those of the extremely metal poor star, CS31082-001, for elements  $i$  with  $Z = 10$ -92.

This work was supported in part by the Japan Society for Promotion of Science(JSPS) Research Fellowships (K.K.), Grants-in-Aid for the Scientific Research from the Ministry of Education, Science and Culture of Japan (No.S14102004, No.14079202, No.17540267), and Grant-in-Aid for the 21st century COE program ‘‘Holistic Research and Education Center for Physics of Self-organizing Systems’’. We are grateful to K. Arai for his carefully reading the manuscript and giving useful comments.

## REFERENCES

Anders, E., & Grevesse, N. 1989, *Geochim. Cosmochim. Acta* 53, 197

Argast, D., Samland, M. Thielemann, F.-K., & Qian, Y.-Z. 2004, *A&A*, 416, 997

Arnould, M. 1976, *A&A*, 46, 117

Arlandini, C., Käppeler, F., Wisshak, K., Gallino, R., Lugaro, M., Busso, M., & Straniero, O. 1999, *ApJ*, 525, 886

Beloborodov, A. M. 2003, *ApJ*, 588, 931

Blinnikov, S. I., Dunina-Barkovskaya, N. V., & Nadyozhin, D. K. 1996, *ApJS*, 106, 171

Burris, D. L., Pilachowski, C. A., Armandroff, T. E., Sneden, C., Cowan, J. J., & Roe, H. 2000, *ApJ*, 544, 302

Clayton, D. D. 1968, *Principles of Stellar Evolution and Nucleosynthesis* (Newyork: MacGraw-Hill).

Di Matteo, T., Perna, R., & Narayan, R. 2002, *ApJ*, 579, 706

Firmani, C., Avila-Reese, V., Ghisellini, G., & Tutukov, A. V. 2004, *ApJ*, 611, 1033

Freiburghaus, C., Rosswog, S., & Thielemann, F.-K. 1999, *ApJ*, 525, L121

Fujimoto, S., Hashimoto, M., Koike, O., Arai, K., & Matsuba, R. 2003a, *ApJ*, 585, 418

Fujimoto, S., Hashimoto, M., Arai, K., & Matsuba, R. 2003b, *Origin of Matter and Evolution of the Galaxies 2003* ed. M. Terasawa et al., pp.344-353 (Singapore: World Scientific).

———. 2004, *ApJ*, 614, 817

———. 2005, *Nucl. Phys.* A758, 47

Fujimoto, S., Kotake, K., Yamada, S., Hashimoto, M., & Sato, K. 2006, preprint, *Astroph/0602457* (*ApJ* accepted)

Fuller, G. M., Fowler, W. A., & Newman, M. J. 1980, *ApJS*, 42, 447

———. 1982, *ApJS*, 48, 279

Galama, T., et al. 1998, *Nature*, 395, 670

Giavalisco, M., et al. 2004, *ApJ*, 600, L103

Granot, J., & Ramirez-Ruiz, E. 2004, *ApJ*, 609, L9

- Hashimoto, M. 1995, *Prog. Theor. Phys.* 94 663.
- Heger, A., Fryer, C. L., Woosley, S. E., Langer, N., & Hartmann, D. H. 2003, *ApJ*, 591, 288
- Hjorth, J., et al. 2003, *Nature*, 423, 847
- Horiguchi, T., Tachibana, T., & Katakura, T. 1996, *Chart of the Nuclides* (Ibaraki: Nucl. Data Center)
- Howard, W. M., Meyer, B. S., & Woosley, S. E. 1991, *ApJ*, 373, L5
- Hurley K., Sari R. & Djorgovski S.G., 2004, to appear in *Compact Stellar X-ray Sources*, eds. W.H.G. Lewin, M. van der Klis, Cambridge Univ. Press (astro-ph/0211620)
- Käppeler, F., Beer, H. and Wisshak, K. 1989, *Rep. Prog. Phys.* 52, 945
- Kinsey, R. R. et al., *The NUDAT/PCNUDAT Program for Nuclear Data, the 9th International Symposium of Capture-Gamma-ray Spectroscopy and Related Topics*, Budapest, Hungary, October (1996)
- Kodama, T., & Takahashi, K. 1975, *Nucl. Phys.* A239 489.
- Kotake, K., Sawai, H., Yamada, S., & Sato, K. 2004, *ApJ*, 608, 391
- Langanke, K., et al. 2003, *Phys. Rev. Lett.*, 90, 241102
- Maeda, K., & Nomoto, K. 2003, *ApJ*, 598, 1163
- Mamdouh, A., Pearson, J.M., Rayet, M., & Tondeur, F. 1999, *Nucl. Phys. A.* 644, 389
- Mamdouh, A., Pearson, J.M., Rayet, M., & Tondeur, F. 2001, *Nucl. Phys. A.* 679, 337
- Mizuno, Y., Yamada, S., Koide, S., & Shibata, K. 2004a, *ApJ*, 606, 395
- Mizuno, Y., Yamada, S., Koide, S., & Shibata, K. 2004b, *ApJ*, 615, 389
- Murakami, T., Yonetoku, D., Umemura, M., Matsumayashi, T., & Yamazaki, R. 2005, *ApJ*, 625, L13
- Nagataki, S., Hashimoto, M., Sato, K., & Yamada, S. 1997, *ApJ*, 486, 1026
- Nishimura, S., Kotake, K., Hashimoto, M., Yamada, S., Nishimura, N., Fujimoto, S., & Sato, K. 2005, preprint, Astro-ph/0504100 (*ApJ* submitted)
- Panov, I.V., Kolbe, E., Pfeiffer, B. Rauscher, T., Kratz, K.-L., & Thielemann, F.-K. 2005, *Nucl. Phys.* A747, 633
- Paczynski, B., & Wiita, P. J. 1980, *A&A*, 88, 23
- Podsiadlowski, P., Mazzali, P. A., Nomoto, K., Lazzati, D., & Cappellaro, E. 2004, *ApJ*, 607, L17
- Proga, D., MacFadyen, A. I., Armitage, P. J., & Begelman, M., C. 2003, *ApJ*, 599, 5
- Pruet, J., Woosley, S. E., & Hoffman, R. D. 2003a, *ApJ*, 586, 1254
- Pruet, J., Thompson, T. A., & Hoffman, R. D. 2004, *ApJ*, 606, 1006
- Qian, S. 2003, *Prog. Part. Nucl. Phys.* 50, 153
- Qian, Y.-Z. & Wasserburg, G. J. 2003, *ApJ*, 588, 1099
- Rayet, M., Arnould, M., Hashimoto, M., Prantzos, N., & Nomoto, K. 1995, *A&A*, 298, 517
- Shen, H., Toki, H., Oyamatsu, K., & Sumiyoshi, K. 1998, *Nucl. Phys. A.*, 637, 435
- Shigeyama, T., & Tsujimoto, T. 1998, *ApJ*, 507, L135
- Stone, J. M., & Norman, M. L. 1992, *ApJS*, 80, 791
- Stone, J. M., & Pringle, J. E. 2001, *MNRAS*, 322, 461
- Staudt, A., Klapdor-Kleingrothaus, H. V. 1992, *Nucl. Phys.* A549 254
- Sumiyoshi, K., Suzuki, H., Otsuki, K., Terasawa, M., & Yamada, S. 2000, *PASJ*, 52, 601
- Sumiyoshi, K., Terasawa, M., Mathews, G. J., Kajino, T., Yamada, S., & Suzuki, H. 2001, *ApJ*, 562, 880
- Terasawa, M., Sumiyoshi, K., Yamada, S., Suzuki, H., & Kajino, T. 2002, *ApJ*, 578, L137

- Totani, T. 2003, ApJ, 598, 1151
- Truran, J. W., Cowan, J. J., Pilachowski, C. A., & Sneden, C. 2002, PASP, 114, 1293
- Yonetoku, D., Murakami, T., Nakamura, T., Yamazaki, R., Inoue, A. K., & Ioka, K. 2004, ApJ, 609, 935
- Wanajo, S., Tamamura, M., Itoh, N., Nomoto, K., Ishimaru, Y., Beers, T. C., & Nozawa, S. 2003, ApJ, 593, 968
- Wasserburg, G. J., Busso, M., & Gallino, R. 1996, ApJ, 466, L109
- Wheeler, J. C., Cowan, J. J., & Hillebrandt, W. 1998, ApJ, 493, L101
- Woosley, S. E., & Howard, W. M., 1978, ApJS, 36, 285
- Woosley, S. E. 1993, ApJ, 405, 273
- Woosley, S. E., & Weaver, T. A. 1995, ApJS, 101, 181
- Zeh, A., Klose, S., & Hartmann, D. H. 2004, ApJ, 609, 952